

Title	Single-particle characterization of biomass burning organic aerosol (BBOA): Evidence for non-uniform mixing of high molecular weight organics and potassium
Authors	Lee, Alex K. Y.;Willis, Megan D.;Healy, Robert M.;Wang, Jon M.;Jeong, Cheol-Heon;Wenger, John C.;Evans, Greg J.;Abbatt, Jonathan P. D.
Publication date	2016-05-04
Original Citation	Lee, A. K. Y., Willis, M. D., Healy, R. M., Wang, J. M., Jeong, C. H., Wenger, J. C., Evans, G. J. and Abbatt, J. P. D. (2016) 'Single-particle characterization of biomass burning organic aerosol (BBOA): evidence for non-uniform mixing of high molecular weight organics and potassium', Atmospheric Chemistry and Physics, 16, pp.5561-5572. doi: 10.5194/acp-16-5561-2016
Type of publication	Article (peer-reviewed)
Link to publisher's version	http://www.atmos-chem-phys.net/16/5561/2016/ - 10.5194/acp-16-5561-2016
Rights	© 2016, the Author(s). This work is distributed under the Creative Commons Attribution 3.0 License. - https://creativecommons.org/licenses/by/3.0/
Download date	2025-07-31 05:19:38
Item downloaded from	https://hdl.handle.net/10468/4176



UCC

University College Cork, Ireland
Coláiste na hOllscoile Corcaigh



Supplement of

**Single-particle characterization of biomass burning organic aerosol (BBOA):
evidence for non-uniform mixing of high molecular weight organics and
potassium**

Alex K. Y. Lee et al.

Correspondence to: A. K. Y. Lee (alexky.lee@utoronto.ca)

The copyright of individual parts of the supplement might differ from the CC-BY 3.0 licence.

Section S1: ACSM measurement

Non-refractory particulate matter (NR-PM) compositions were measured using an aerosol chemical speciation monitor (ACSM, Aerodyne Research Inc.) at a 30 minute time resolution. The ACSM can provide mass concentrations of organics, sulfate, nitrate, ammonium and chloride for aerosol with vacuum aerodynamic diameters smaller than 1 μm (PM_{10}). The instrument is described in detail elsewhere (Ng et al., 2011). Briefly, ambient particles are sampled through an aerodynamic focusing lens. The particles in the narrow beam impact and volatilize on a tungsten vaporizer heated at $\sim 600^\circ\text{C}$. The vapors are ionized by electron impact ionization and analyzed by a quadrupole mass spectrometer.

The ACSM was calibrated for the inlet flow rate, nitrate ionization efficiency (IE_{NO_3}) and relative ionization efficiencies (RIE) of ammonium and sulfate. Mono-dispersed NH_3NO_3 and $(\text{NH}_4)_2\text{SO}_4$ aerosol was introduced for the ionization calibration using an atomizer (3076, TSI), a differential mobility analyzer (DMA, 3081, TSI), and a condensation particle counter (CPC, 3786, TSI). The average and standard deviation of the IE_{NO_3} for nitrate was 2.88×10^{-11} and 8.19×10^{-12} respectively. The default RIE value for organics (1.4) was used. Additionally, an internal naphthalene source and the N_2 beam signal were used to adjust for the system stability. To compensate for particle losses in the ACSM, a collection efficiency (CE) of 0.5 is applied for data correction (Canagaratna et al. 2007).

Section S2 Positive Matrix Factorization (PMS) of AMS data

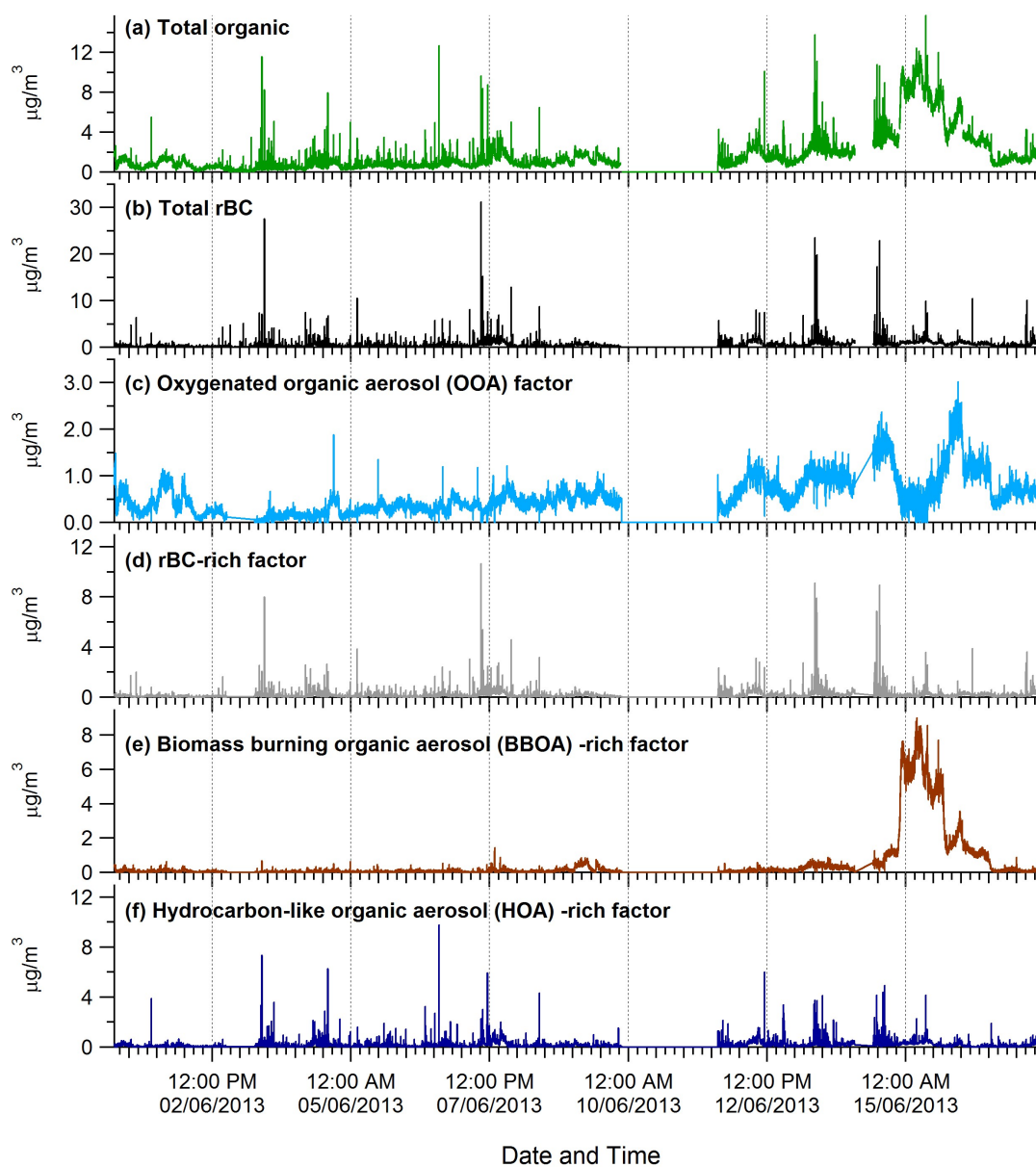


Figure S1: Time series of (a) ensemble organic aerosol and (b) refractory black carbon mass loadings. Positive matrix factorization (PMF) results for ensemble data (c) to (f): (c) background oxygenated organic aerosol (OOA), (d) rBC-rich particles (e) biomass burning organic aerosol (BBOA), and (f) hydrocarbon-like organic aerosol (HOA) rich particles.

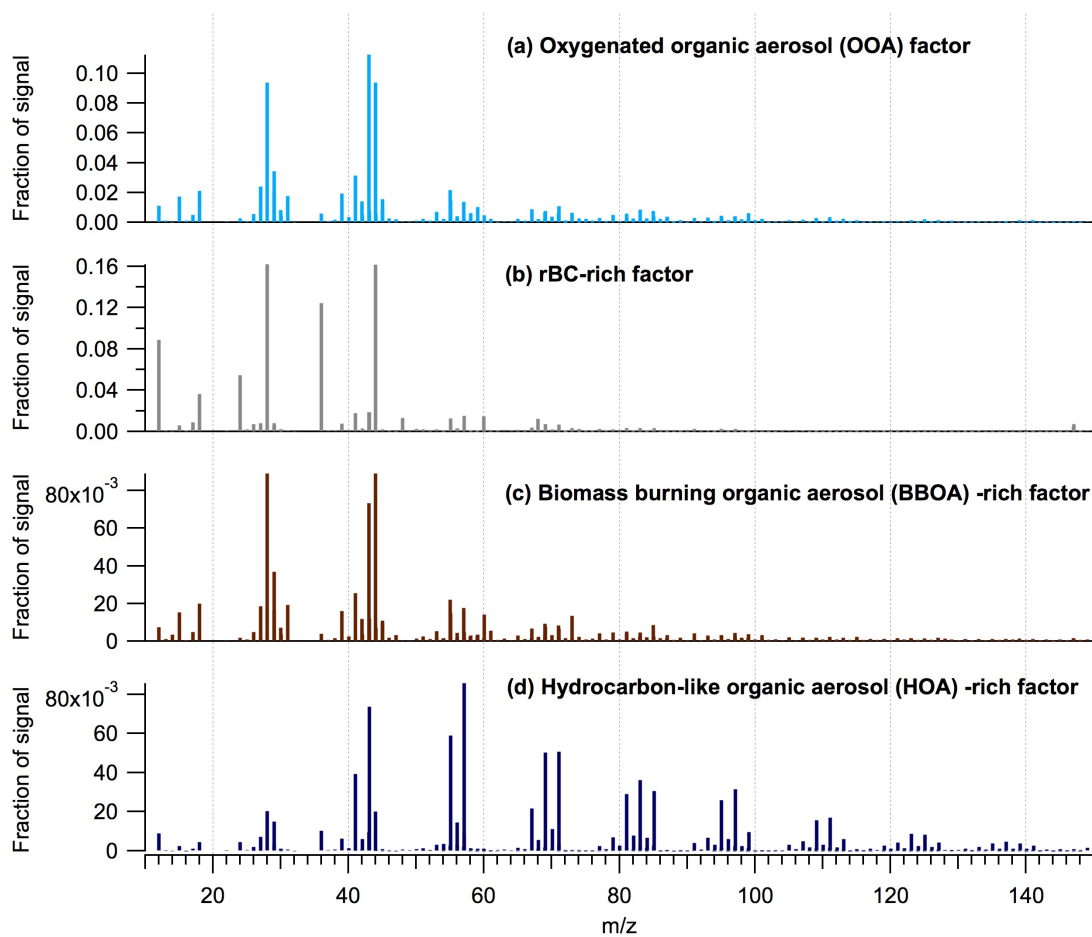


Figure S2: Ensemble data: Mass spectra of the four-factor PMF solution. The four factors represent (a) background oxygenated organic aerosol (OOA), (b) rBC-rich particles (c) biomass burning organic aerosol (BBOA), and (d) hydrocarbon-like organic aerosol (HOA) rich particles.

Section S3: Size distributions of total ion and potassium signals of individual particles

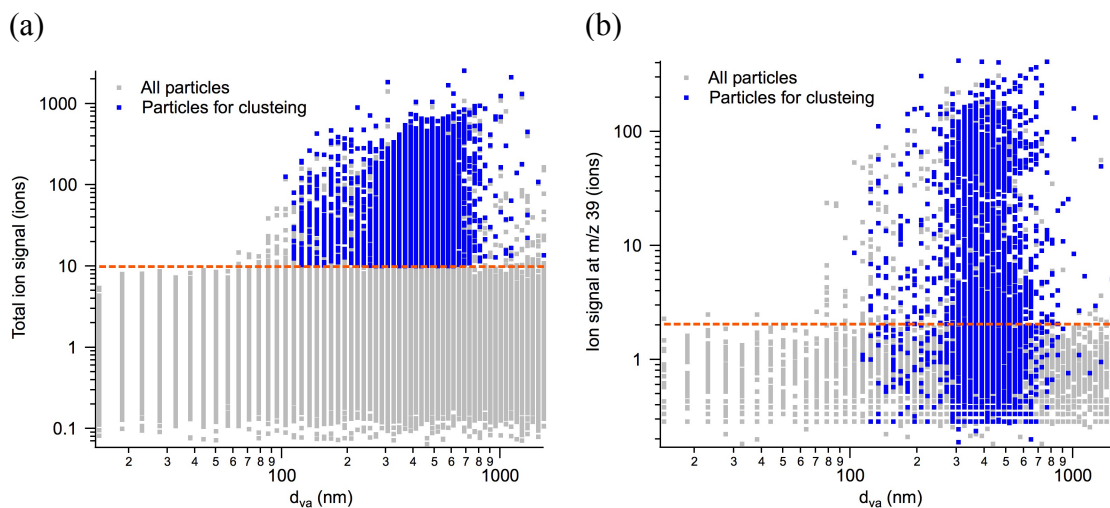


Figure S3: Size distributions of (a) total ion signal and (b) m/z 39 (potassium) signal of individual particles. Orange dashed lines represent the ion threshold values (i.e., 10 and 2 ions for total ion and m/z 39, respectively).

Section S4: Estimation of BBOA coating thickness

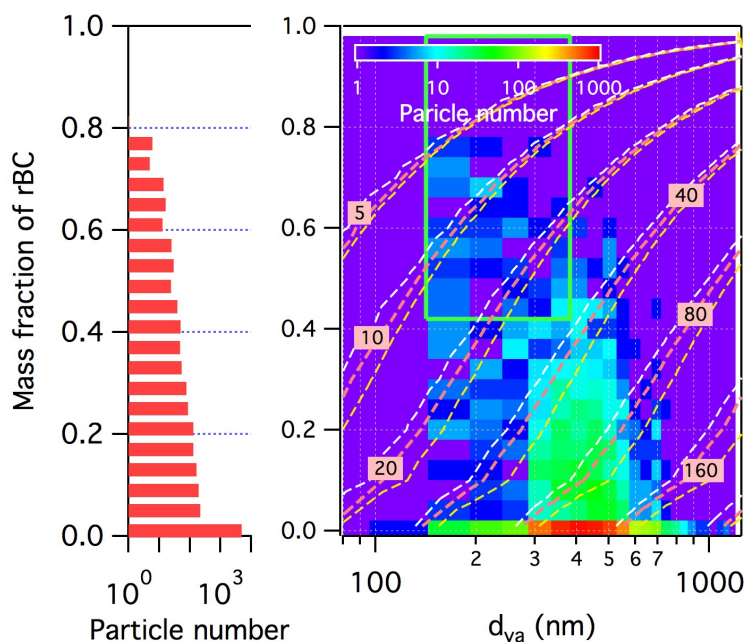


Figure S4: Two-dimensional histogram (mass fraction of rBC vs. particle aerodynamic diameter) of all BBOA-related particle classes. The color scale represents the number of particles in the particle classes. The dashed lines represent the physical thickness (nm) of organic coating on rBC-containing particles determined by a core-shell structure model (assuming uniform coating, spherical particle shape, and density of BBOA of 1.3 g/cm³, respectively). White, red and yellow dashed lines represent calculation results by assuming effective density of rBC of 0.3, 0.8 and 1.4 g/cm³, respectively. Note that most of the rBC-rich particles fall into the area covered by the green rectangle.

Section 5: Ternary plots of rBC, Org_{BC} and K for other BBOA-related particle types

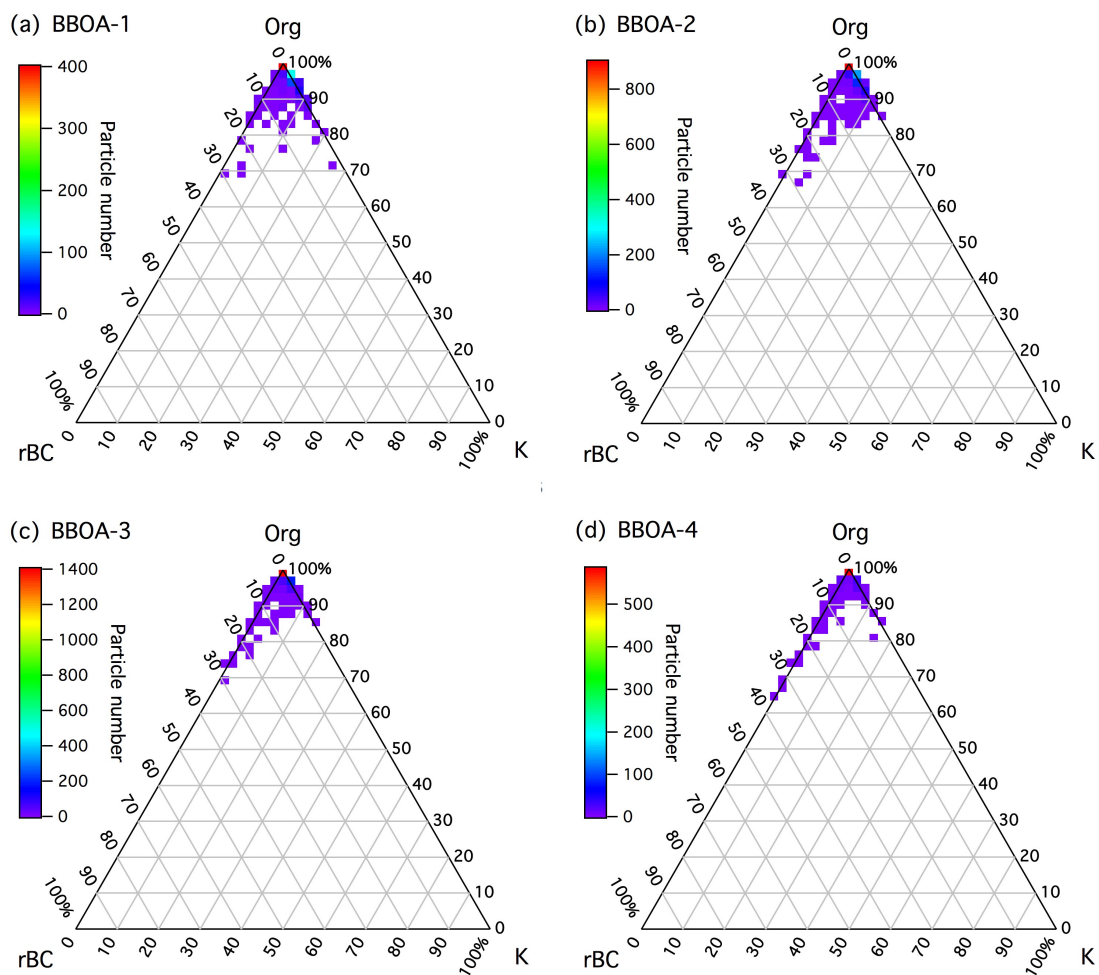


Figure S5: Ternary plots of rBC, Org_{BC} and K ion signal for (a) BBOA-1, (b) BBOA-2, (c) BBOA-3 and (d) BBOA-4.

Section S5: Estimation of the mass fraction of total BBOA retained in the thermo-processed particles

Figure S6a displays the time series for particle volume of ambient and thermo-processed aerosols (with the correction included for the particle transmission efficiency of the thermodenuder) measured by the SMPS. The evaporated fraction of aerosol volume (equivalent to aerosol mass if particle density is constant) in the thermodenuder was calculated from the difference between the two sampling channels and the result is shown in Figure S6b (black open circles). The removal efficiency of aerosol volume was 60-80% for the majority of the sampling period and decreased to ~40% on June 15, when the site was most heavily impacted by the wildfire emissions. The remaining particle volume can be due to the presence of refractory aerosol species (e.g., rBC and mineral dust) and low-volatility NR-PM that cannot be removed efficiently by the thermodenuder. Note that Healy et al. (2015) determined that the removal efficiency of scattering aerosol at 405 nm was approximately 60% on June 15 and above 80% for other periods based on the PASS-3 measurement.

The relatively low removal efficiency of BBOA aerosol volume during the BB period suggests the presence of low-volatility BBOA components, which can be further quantified using the PMF analysis of aerosol mass spectrometry measurements. Given that the LS-SP-AMS without the tungsten vaporizer only detected rBC and NR-PM_{rBC}, the total aerosol mass (i.e., rBC and non-refractory inorganic and organic components) was re-calculated based on correlations of PMF factors obtained from the LS-SP-AMS and ACSM measurements. This approach is used to calculate the total aerosol mass instead of using the ACSM data directly because the ACSM was not sampling from June 9, 20:00 to June 11, 15:00 and from June 13, 17:30 to June 15, 18:30. Collection efficiency of 0.5 was used to correct the ACSM data.

The LS-SP-AMS data accounted for approximately 46% ($R^2 = 0.87$), 31% ($R^2 = 0.57$) and 19% ($R^2 = 0.13$) of BBOA, oxygenated organic aerosol (OOA), and hydrocarbon-like organic aerosol (HOA) factors of the ACSM measurements, respectively (Figure S7). Note that the weak correlation of HOA factors does not significantly impact the

calculation result because of a relatively low mass loading of HOA. The correction factors for NH_4 , NO_3 and SO_4 are assumed to be 31% (i.e. the same value as for OOA) due to the fact that these secondary inorganic species and OOA are generally internally mixed in accumulation mode particles (Lee et al. 2015). Using all these parameters, the total ambient aerosol mass was determined accordingly, and the calculated result is shown in Figure S6c (green area).

Figure S6b illustrates that the estimated loss of aerosol mass cannot reproduce the SMPS observation within the BB period if rBC was the only component that cannot be removed by the thermodenuder (i.e. compare blue line in Figure S6b with the black open circle in Figure S6b). In contrast, assuming that 1) rBC represented all non-volatile components, 2) 60% of the total BBOA was of extremely low volatility, and 3) other aerosol components were completely evaporated in the thermodenuder, the estimation was able to capture most of the variation observed by the SMPS measurements throughout the entire sampling period (i.e. compare orange line in Figure S6b with the black open circle in Figure S6b). The calculation suggests that approximately 60% of total BBOA was not removed by the thermodenuder under the specified operating conditions.

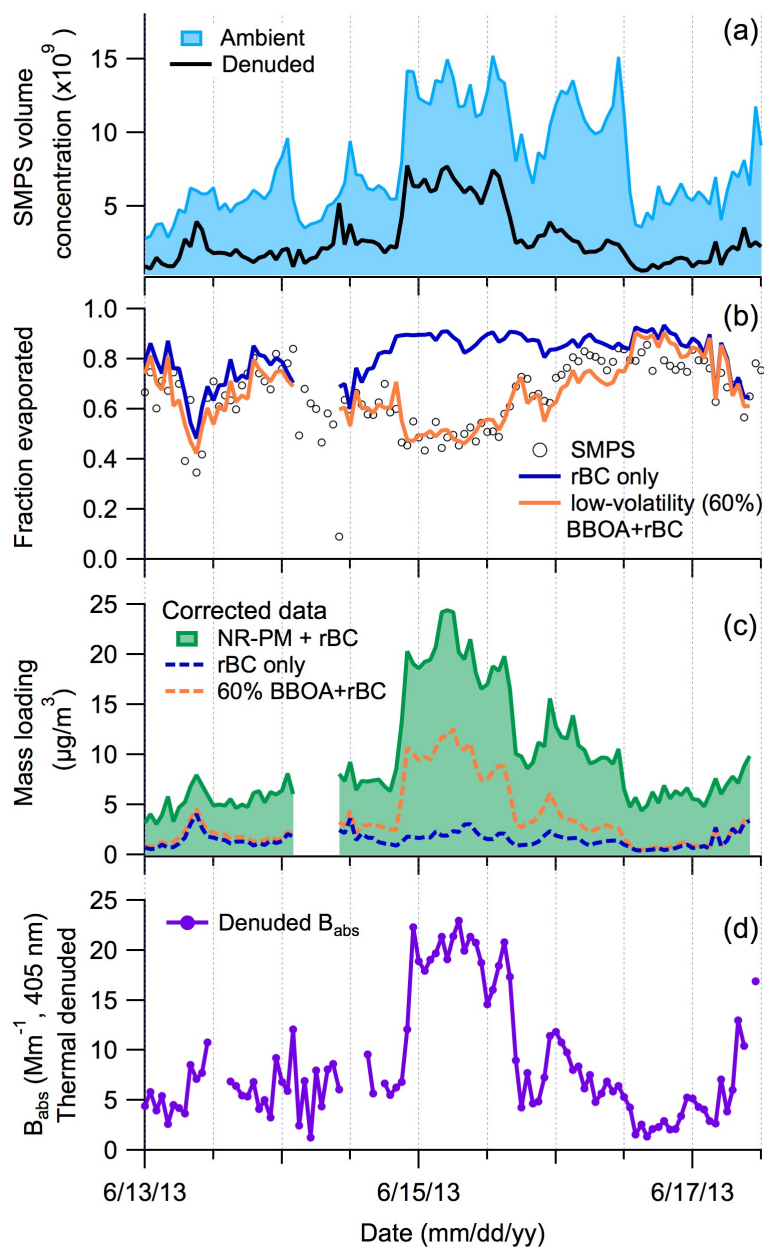


Figure S6: Time series of a) aerosol volume measured by SMPS, b) the evaporated fraction of aerosol volume or mass in the thermodenuder, c) calculated total aerosol mass (rBC + NR-PM), rBC mass (with CE correction), and rBC + 60% of total BBOA, and d) aerosol absorption at the wavelength of 405 nm of thermo-denuded particles.

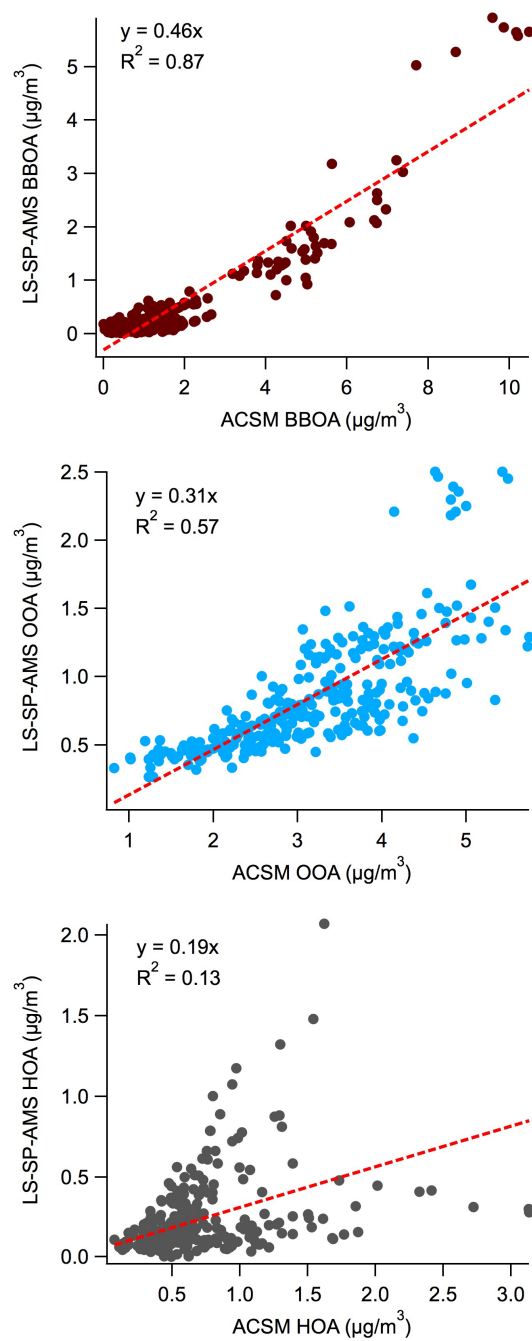


Figure S7: Correlations of LS-SP-AMS and ACSM measurements: BBOA (top), OOA (middle) and HOA (bottom).

Section S6: ATOFMS mass spectra

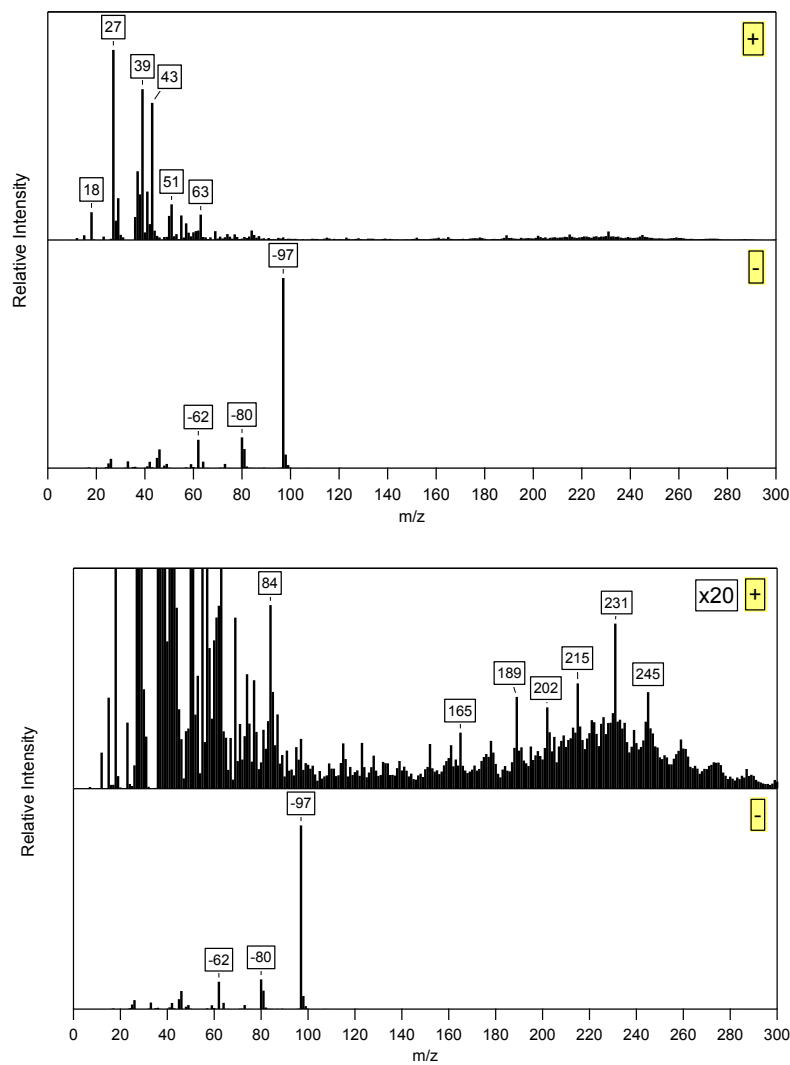


Figure S8: ATOFMS average mass spectrum (positive and negative ion modes) for single particles with signals attributable to HMW classified through cluster analysis. The positive ion mass spectrum relative intensity axis has been rescaled in the bottom panel to highlight HMW ions of interest. The signal at m/z 202 is consistent with the molecular ion for fluoranthene and/or pyrene (Gross et al. 2000). A signal at m/z 165 has been previously identified as a fragment ion from substituted phenanthrene ($C_{13}H_9^+$) (Bente et al. 2009). Analogous tentative assignments for m/z 189 and 215 are thus the aromatic fragment ions $C_{15}H_9^+$ and $C_{17}H_{11}^+$, respectively. The identity of 231 and 245 are unknown.

References:

- Bente, M., et al.: Thermal Desorption–Multiphoton Ionization Time-of-Flight Mass Spectrometry of Individual Aerosol Particles: A Simplified Approach for Online Single-Particle Analysis of Polycyclic Aromatic Hydrocarbons and Their Derivatives, *Anal. Chem.*, 81, 2525-2536, 10.1021/ac802296f, 2009.
- Canagaratna, M. R., Jayne, J. T., Jimenez, J. L., Allan, J. D., Alfarra, M. R., Zhang, Q., Onasch, T. B., Drewnick, F., Coe, H., Middlebrook, A., Delia, A., Williams, L. R., Trimborn, A. M., Northway, M. J., DeCarlo, P. F., Kolb, C. E., Davidovits, P. and Worsnop, D. R.: Chemical and microphysical characterization of ambient aerosols with the aerodyne aerosol mass spectrometer, *Mass Spectrom. Rev.*, 26, 185-222, 2007.
- Lee, A. K. Y., Willis, M. D., Healy, R. M., Onasch, T. B., and Abbatt, J. P. D.: Mixing state of carbonaceous aerosol in an urban environment: single particle characterization using the soot particle aerosol mass spectrometer (SP-AMS), *Atmos. Chem. Phys.*, 15, 1823-1841, 2015.
- Gross, D. S., et al.: Relative Sensitivity Factors for Alkali Metal and Ammonium Cations in Single-Particle Aerosol Time-of-Flight Mass Spectra, *Anal. Chem.*, 72, 416-422, 2000.
- Healy, R. M., Wang, J. M., Jeong, C. -H., Lee, A. K. Y., Willis, M. D., Jaroudi, E., Zimmerman, N., Hilker, N., Murphy, M., Eckhardt, S., Stohl, A., Abbatt, J. P. D., Wenger, J. C., and Evans, G. J.: Light-absorbing properties of ambient black carbon and brown carbon from fossil fuel and biomass burning sources, *J. Geophys. Res.-Atmos.*, 120, 6619-6633, 2015.
- Ng, N. L., Herndon, S. C., Trimborn, A., Canagaratna, M. R., Croteau, P. L., Onasch, T. B., Sueper, D., Worsnop, D. R., Zhang, Q., Sun, Y. L., and Jayne, J. T.: An Aerosol Chemical Speciation Monitor (ACSM) for Routine Monitoring of the Composition and Mass Concentrations of Ambient Aerosol, *Aerosol Sci. Technol.*, 45, 780-794, 2011.